

# Analytical Modeling and Design Optimization of Linear Synchronous Motor With Stair-Step-Shaped Magnetic Poles for Electromagnetic Launch Applications

Nariman Roshandel Tavana, *Student Member, IEEE*, Abbas Shoulaie, and Venkata Dinavahi, *Senior Member, IEEE*

**Abstract**—In this paper, a stair-step-shaped magnetic pole structure is proposed to use in a permanent-magnet linear synchronous motor (PMLSM) for its application in an electromagnetic launch system. The aim of this configuration is to shape the air-gap flux density distribution produced by poles to be as close to a sine waveform as possible for the reduction of thrust ripple and the increase of motor controllability. An analytical model is derived for the PMLSMs by solving Maxwell equations and applying the superposition theorem for calculating the magnetic field, electromotive force, and thrust/torque of the motor. Magnet dimensions are then optimized using the analytical method and genetic algorithm, where the reduction of air-gap flux density harmonics is considered as the optimization target. Finally, the effectiveness of the proposed technique to enhance the motor performance is investigated by a time-stepping transient finite-element method. The results show an improvement in the optimal motor performance.

**Index Terms**—Analytical modeling, finite-element methods (FEMs), permanent-magnet linear synchronous motor (PMLSM), stair-step-shaped magnetic pole (S<sup>3</sup>MP).

## NOMENCLATURE

$J_M$	Equivalent magnetization current vector.
$a_y$	Unit vector in the $y$ -direction.
$H$	Magnetic field intensity.
$B$	Magnetic field density.
$F$	Thrust force.
$e$	Induced electromotive force (EMF).
$\varphi$	Flux linkage of a winding.
$L$	Motor width.
$g$	Mechanical air-gap length.
$k_{wn}$	Winding factor of the $n$ th harmonic.
$p_f$	Coil packing factor.
$P$	Number of pole pairs.
$l_m$	Magnet height.

$l_w$	Winding height.
$w_m$	Magnet width.
$w_w$	Winding width.
$\tau$	Pole pitch.
$\tau_{wp}$	Winding pitch.
$J$	Current density.
$B_r$	Remanence.
$x_0$	Load angle.
$v_s$	Synchronous speed.

## I. INTRODUCTION

**E**LECTROMAGNETIC launcher (EML) is a kind of technology used to develop thrust force and launch heavy loads. It can be utilized for various industries including military, aerospace, and civil applications [1], [2]. Due to their high efficiency, compact structure, high thrust-to-current ratio, fast dynamic response, simple mechanical construction, high power density, and easy maintenance and control [3]–[6], permanent-magnet (PM) linear synchronous motors (PMLSMs) are appropriate for linear electromagnetic launcher. Additionally, these advantages of PMLSMs in EML have enabled it to supplant the steam catapult system [7] which has been used with low overall efficiency for over 50 years [8]. Among the various PMLSM types, slotted topologies suffer from detent force due to the slots of the primary part and finite length of the moving part. Detent force increases thrust fluctuation and decreases motor controllability. On the other hand, in some applications such as space platforms and electromagnetic guns, a high operational accuracy of the motor is required. A suitable solution is a slotless topology offering relatively low thrust ripple and no detent force [9], [10]. A slotless PMLSM is usually driven with sinusoidal currents to satisfy applications that require less mechanical vibration. Ideally, it should have a sinusoidal air-gap flux density distribution, a sinusoidal current waveform, and a quasi-sinusoidal distribution of stator conductors [11]. Therefore, the flux density distribution of PM poles plays a crucial role in their performance, and a nonsinusoidal flux density distribution with significant harmonics leads to performance degradation.

Different methods have so far been proposed for the shaping of PM poles to produce a sine magnetic field and to improve the PM motor efficiency. One method is the magnet-arc-shaping technique [12]–[14]. In this model, the outer surface of the

Manuscript received August 26, 2011; revised October 20, 2011 and November 23, 2011; accepted November 29, 2011. Date of publication December 29, 2011; date of current version February 10, 2012.

N. R. Tavana and V. Dinavahi are with the Department of Electrical and Computer Engineering, University of Alberta, Edmonton, AB T6G 2V4, Canada (e-mail: roshande@ualberta.ca; dinavahi@ualberta.ca).

A. Shoulaie is with the Department of Electrical Engineering, Iran University of Science and Technology, Tehran 16846-13114, Iran (e-mail: shoulaie@iust.ac.ir).

Color versions of one or more of the figures in this paper are available online at <http://ieeexplore.ieee.org>.

Digital Object Identifier 10.1109/TPS.2011.2178616

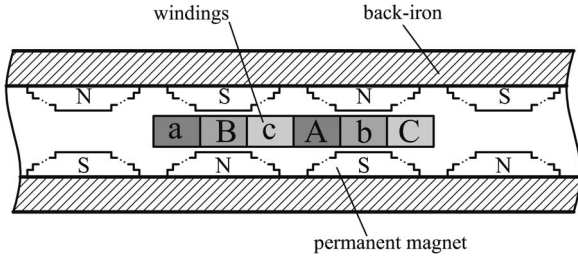


Fig. 1. Topology of a double-sided PMLSM with  $S^3$ MPs.

poles in a PM motor is considered as a part of a cylinder. However, this method increases the complexity and cost of manufacturing. Another method is pulsewidth modulation (PWM) [15], [16]. In this configuration, the block magnets are arranged similar to PWM signals used to switch power electronic devices. This technique reduces the flux density of the PM pole as well as the machine thrust or torque. Moreover, it is very hard to implement because placing the segments of a divided PM pole in one direction of magnetization vectors near to each other in a PM motor with short pole pitch is quite difficult. The third method is the modular PM pole technique [17]. In this model, the pole consists of three or more magnet pieces with different types and specifications. Unfortunately, that is why this technique increases the complexity and cost of manufacturing of PM machines. The fourth method is to use the Halbach magnetized topology [18]–[20]. This method needs many magnet pieces with different sizes and directions of magnetization. Thus, it uses excessive amount of PM material, leading to a high production cost. It is worth mentioning that some of these methods are also used for reduction of cogging force [21]–[25].

This paper proposes a new structure for the magnetic poles in the PMLSM to shape their air-gap flux density distribution. The proposed pole configuration is called the stair-step-shaped magnetic pole ( $S^3$ MP). The  $S^3$ MPs develop high thrust or torque and reduce flux density as well as EMF harmonics substantially. Furthermore, the design complexity of this method is considerably less than those of the aforementioned methods. In this paper, a PMLSM incorporating the proposed  $S^3$ MPs is presented as a case study, and then, an analytical method is used for its modeling. Moreover, the finite-element method (FEM) is employed to evaluate the accuracy of the analytical modeling. Finally, pole shape optimization is carried out using the developed analytical model, together with a genetic algorithm. The comparison between the initial motor and optimized motor performances proves the validity of modeling and design optimization.

## II. ANALYTICAL ANALYSIS OF A PM MACHINE WITH $S^3$ MPs

### A. Machine Topology

The  $S^3$ MPs can be used in different topologies of PM motors. This paper focuses on modeling and design optimization of a double-sided PMLSM topology with the proposed  $S^3$ MPs shown in Fig. 1 which is appropriate for EML. The practical issues in implementing this type of machine can be found in [26]–[29].

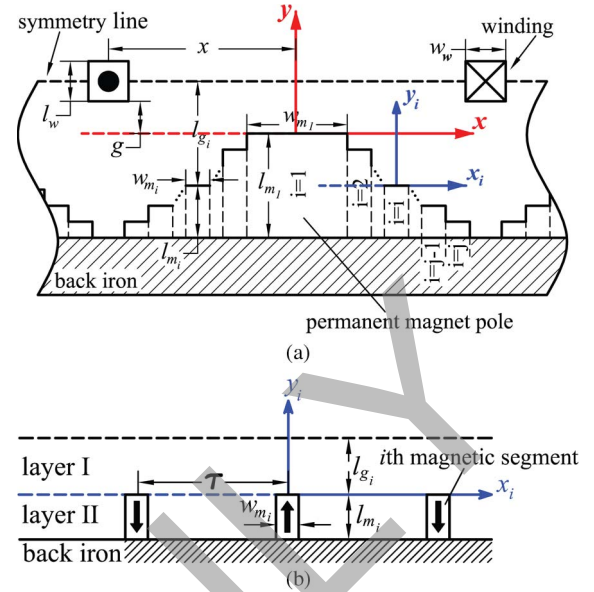


Fig. 2. Magnetic field analysis model for the PM: (a) Simplified model and (b) field regions.

### B. Field Distribution due to PM Source

In order to establish analytical solutions for the magnetic field distribution in the foregoing machine topology, the following assumptions are made [1], [30].

- 1) The length of the motor is extended to infinity.
- 2) The permeability of the iron core is infinite.
- 3) The PMs have a linear demagnetization characteristic, and their permeability is equal to the permeability of free space.

As the surfaces of PM poles have different heights, the solution of Maxwell equations for calculating the magnetic field becomes difficult. The magnetic field should be calculated by splitting the magnet piece into  $2j - 1$  segments, as shown in Fig. 2(a). Therefore, a layer model can be used to solve the Maxwell equations in each magnetic segment for the prediction of the field distribution.

Consequently, the magnetic field analysis due to the  $i$ th magnetic segment is confined to two layers: the air space/winding and the PM layer. Fig. 2(b) shows the field regions of the  $i$ th segment. The governing field equations in terms of the magnetic vector potential for the  $i$ th segment lead to Laplace and Poisson equations as follows [31]:

$$\begin{cases} \nabla^2 A_{I_i} = 0, & \text{in layer I} \\ \nabla^2 A_{II_i} = -\mu_0 \mathbf{J}_{M_i}, & \text{in layer II} \end{cases} \quad (1)$$

where  $\mathbf{J}_{M_i} = \nabla \times \mathbf{M}_i$  and  $\mathbf{M}_i$  is the magnetization vector of the  $i$ th magnetic segment given by

$$\mathbf{M}_i = M_{y_i} \mathbf{a}_y \quad (2)$$

where  $M_{y_i}$  denotes the component of  $\mathbf{M}_i$  in the  $y$ -direction. The distribution of  $M_{y_i}$  can be expressed as the Fourier series

$$M_{y_i} = \sum_{n=1,3,\dots}^{\infty} P_n \sin\left(\frac{m_n w_{m_i}}{2}\right) \cos(m_n x_i) \quad (3)$$

where  $P_n = 4B_r/n\pi\mu_0$  and  $m_n = n\pi/\tau$ . The boundary conditions to be satisfied by the solution to (1) are

$$\begin{aligned} H_{Ix_i}|_{y_i=l_{g_i}} &= 0 & H_{IIx_i}|_{y_i=-l_{m_i}} &= 0 \\ H_{Ix_i}|_{y_i=0} &= H_{IIx_i}|_{y_i=0} & B_{Iy_i}|_{y_i=0} &= B_{IIy_i}|_{y_i=0} \end{aligned} \quad (4)$$

where  $l_{g_i}$  is the effective air-gap length of the  $i$ th segment given by

$$l_{g_i} = g + l_w/2 + l_{m_1} - l_{m_i}. \quad (5)$$

By solving (1), the tangential and normal components ( $B_{x_i}$  and  $B_{y_i}$ ) of the flux density produced by the  $i$ th segment in the air gap are provided from the curl of  $\mathbf{A}_{I_i}$  as follows:

$$\begin{aligned} B_{Ix_i}(x_i, y_i) &= - \sum_{n=1,3,\dots}^{\infty} m_n [a_{In_i} \sinh(m_n y_i) \\ &\quad + b_{In_i} \cosh(m_n y_i)] \sin(m_n x_i) \end{aligned} \quad (6)$$

$$\begin{aligned} B_{Iy_i}(x_i, y_i) &= \sum_{n=1,3,\dots}^{\infty} m_n [a_{In_i} \cosh(m_n y_i) \\ &\quad + b_{In_i} \sinh(m_n y_i)] \cos(m_n x_i) \end{aligned} \quad (7)$$

where  $a_{In_i}$  and  $b_{In_i}$  are determined as

$$\begin{aligned} a_{In_i} &= \frac{(e^{m_n l_{m_i}} - e^{-m_n l_{m_i}})(e^{m_n l_{g_i}} - e^{-m_n l_{g_i}})}{(e^{m_n(l_{g_i}+l_{m_i})} - e^{-m_n(l_{g_i}+l_{m_i})})} \\ &\quad \times \left( \frac{P_n \mu_0}{2m_n} \sin\left(\frac{m_n w_{m_i}}{2}\right) \right) \end{aligned} \quad (8)$$

$$b_{In_i} = \frac{(e^{-m_n l_{g_i}} - e^{m_n l_{g_i}})}{(e^{m_n l_{g_i}} + e^{-m_n l_{g_i}})} a_{In_i}. \quad (9)$$

As the soft magnetic parts are assumed to be infinitely permeable and all materials behave linearly [17], therefore, the resultant air-gap flux density is obtained in terms of  $x$  and  $y$  components by using the superposition theorem as

$$B_x(x, y) = B_{Ix_1} + \sum_{i=2}^j B_{Ix_i}(XW(x, i), y - l_{m_1} + l_{m_i}) \quad (10)$$

$$B_y(x, y) = B_{Iy_1} + \sum_{i=2}^j B_{Iy_i}(XW(x, i), y - l_{m_1} + l_{m_i}) \quad (11)$$

where

$$XW(x, i) = \begin{cases} x \pm \frac{w_{m_1}}{2} \pm \frac{w_{m_2}}{2}, & \text{if } i = 2 \\ x \pm \frac{w_{m_1}}{2} \pm \frac{w_{m_i}}{2} \pm \sum_{j=3}^i w_{m_{j-1}}, & \text{if } i > 2. \end{cases} \quad (12)$$

### C. EMF Calculation

The total flux linkage of a distributed multicoil phase winding caused by the  $i$ th magnetic segment can be obtained as

$$\begin{aligned} \varphi_i(x_i) &= \oint_s B_{Iy_i} \cdot ds = \int_0^L \int_{x_i-\tau_{wp}}^{x_i} B_{Iy_i} dx dz \\ &= \sum_{n=1,3,\dots}^{\infty} \phi_{n_i} \cos m_n \left( x_i - \frac{\tau_{wp}}{2} \right) \end{aligned} \quad (13)$$

where

$$\begin{aligned} \phi_{n_i} &= \frac{8PLp_f k_{wn} N_c}{l_w} \sin\left(\frac{m_n \tau_{wp}}{2}\right) \\ &\quad \times \int_{g+l_{m_1}-l_{m_i}}^{g+l_w/2+l_{m_1}-l_{m_i}} [a_{In_i} \cosh(m_n y_i) + b_{In_i} \sinh(m_n y_i)] dy. \end{aligned} \quad (14)$$

Using Faraday's law, the induced EMF due to the  $i$ th segment is given by

$$e_i(x_i) = -\frac{d\varphi_i}{dt} = -v_s \sum_{n=1,3,\dots}^{\infty} \phi_{n_i} m_n \sin m_n \left( x_i - \frac{\tau_{wp}}{2} \right). \quad (15)$$

Thus, the EMF produced by all magnetic segments can be expressed as follows:

$$e(x) = e_1 + \sum_{i=2}^j e_i(XW(x, i)). \quad (16)$$

### D. Thrust Prediction

The average thrust force exerted on the armature resulting from the interaction between the winding current and the fundamental component of the flux density  $B_{y1}$  produced by poles is given by

$$F_{avg} = - \int_V J_z \times B_{y1} dV. \quad (17)$$

Assume that each coil side on the armature occupies areas bounded by  $x_1 = x - w_w/2$ ,  $x_2 = x + w_w/2$ ,  $y_1 = g$ , and  $y_2 = g + l_w$ . The thrust force exerted on each coil side due to the  $i$ th magnetic segment can be obtained from the following integration [32]:

$$F_i(x_i) = 2 \int_{x_i-w_w/2}^{x_i+w_w/2} \int_{g+l_{m_1}-l_{m_i}}^{g+l_w/2+l_{m_1}-l_{m_i}} (LJ B_{y1}) dx dy \quad (18)$$

which can be written as

$$F_i(x_i) = K_i \sin(m_1 x_i) \quad (19)$$

where  $K_i$  is given by

$$K_i = 4LJp_f k_{w1} \sin\left(\frac{m_1 w_w}{2}\right) \times \int_{g+l_{m_1}-l_{m_i}}^{g+l_w/2+l_{m_1}-l_{m_i}} [a_{I1_i} \cosh(m_1 y_i) + b_{I1_i} \sinh(m_1 y_i)] dy. \quad (20)$$

Therefore, the force  $F_{1ph_i}$  exerted on a phase winding comprising a number of series-connected coils is obtained as

$$F_{1ph_i}(x_i) = T_i \sin m_1 \left(x_i - \frac{\tau_{wp}}{2}\right) \quad (21)$$

where  $T_i$  is defined as the thrust constant of the essential component and is given by

$$T_i = 2PK_i \cos\left(\frac{m_1 \tau_{wp}}{2}\right). \quad (22)$$

For a three-phase machine carrying balanced sinusoidally time-varying currents, the average thrust force due to the  $i$ th magnetic segment is obtained from

$$F_{3ph_i}(x_i) = F_{A_i}(x_i) + F_{B_i}(x_i) + F_{C_i}(x_i) \quad (23)$$

$$F_{3ph_i} = \frac{3}{2} T_i \sin\left(\frac{\pi}{\tau} x_{0_i}\right). \quad (24)$$

Therefore, the average thrust force due to all magnetic segments or S<sup>3</sup>MPs is given by

$$F_{\text{avg}} = \frac{3}{2} T_1 \sin\left(\frac{\pi}{\tau} x_0\right) + \sum_{i=2}^j \frac{3}{2} T_i \sin\left(\frac{\pi}{\tau} (XW(x_0, i))\right). \quad (25)$$

### E. Comparison With FEM

The validity of the analytical results for the calculation of the magnetic field, EMF, and thrust force in the PM machines with S<sup>3</sup>MPs greatly depends on the accuracy of the analytical model. However, the analytical model is based on some simplifying assumptions such as ignoring saturation and considering an infinite motor length. Thus, it is necessary to evaluate the extent of model accuracy. In this section, a 2-D nonlinear time-stepping transient FEM is employed to validate the model. The relative movement is taken into account in the FEM by using a time-stepping transient analysis and the Lagrange multiplier method [10]. The flowchart of the FEM is shown in Fig. 3.

In this section, the proposed analytical model is applied to a PMLSM with two-step PM poles whose parameters are listed in Table I. This case is chosen for simplicity without loss of generality. The results can be extended to any other pole configurations with more steps.

A graphical representation of the flux lines and the flux density distribution from FEM in the analyzed motor are shown in Figs. 4 and 5, respectively.

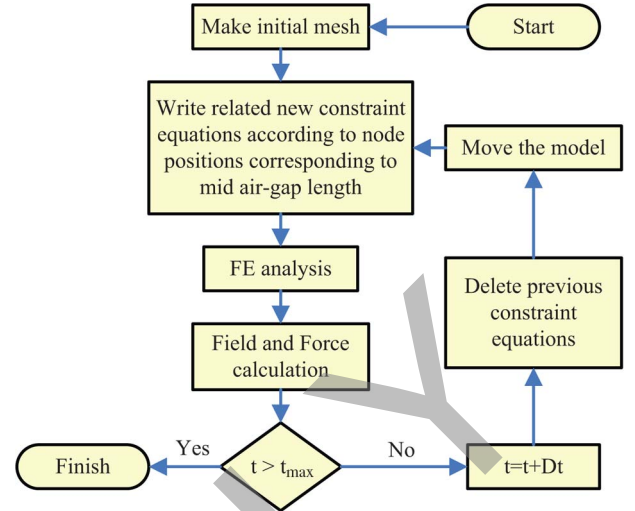


Fig. 3. Flowchart of the finite-element analysis for the PMLSM.

TABLE I  
PARAMETERS OF THE INITIAL PMLSMS

Parameter	Motor Types					
	Conventional Poles	Two-step S <sup>3</sup> MPs		Three-step S <sup>3</sup> MPs		
$l_m$ (mm)	4.4	$l_{m_1}$	5	$l_{m_1}$	5.8	5.2
		$l_{m_2}$	3.1	$l_{m_2}$	3.5	3.5
$w_m$ (mm)	34	$w_{m_1}$	22.6	$w_{m_1}$	18.8	18.8
		$w_{m_2}$	8.3	$w_{m_2}$	2.4	4.4
$\tau$ (mm)			42			
$l_w$ (mm)			6			
$w_w$ (mm)			14			
$J$ (A/mm <sup>2</sup> )			5			
$B_r$ (T)			1.13			
$g$ (mm)			1			

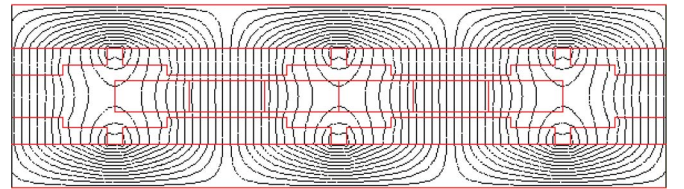


Fig. 4. Magnetic flux lines in the PMLSM.

Fig. 6 shows the comparisons between the normal and tangential components of the open-circuit flux density distributions computed by the analytical method and FEM as functions of the  $x$  position at the center of the mechanical air gap. It is seen that the FEM accurately verifies the analytical method.

A comparison of the EMF waveforms per turn for a constant armature speed of 2.1 m/s obtained by the analytical method and FEM is shown in Fig. 7. Again, a close agreement between the results of the analytical method and FEM is observed.

Fig. 8 shows a comparison of the analytically predicted and finite-element-calculated thrust force distributions with respect to the mover position. It is seen that the analytical prediction agrees well with the finite-element solution; the slight discrepancy is due mainly to the effect of core saturation, which is neglected in the analytical model.

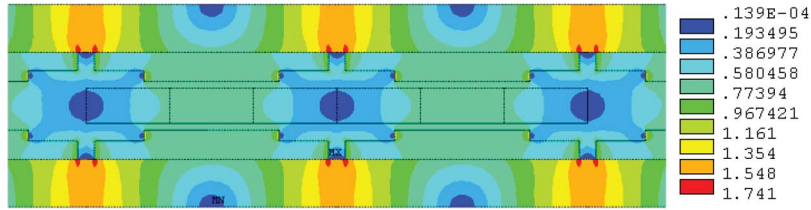
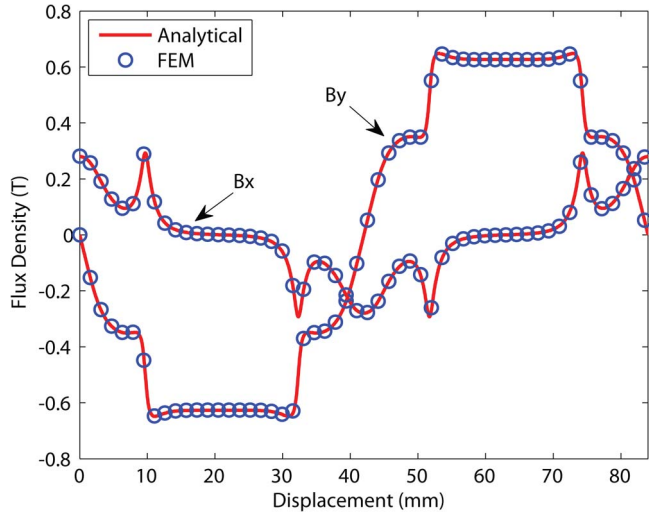
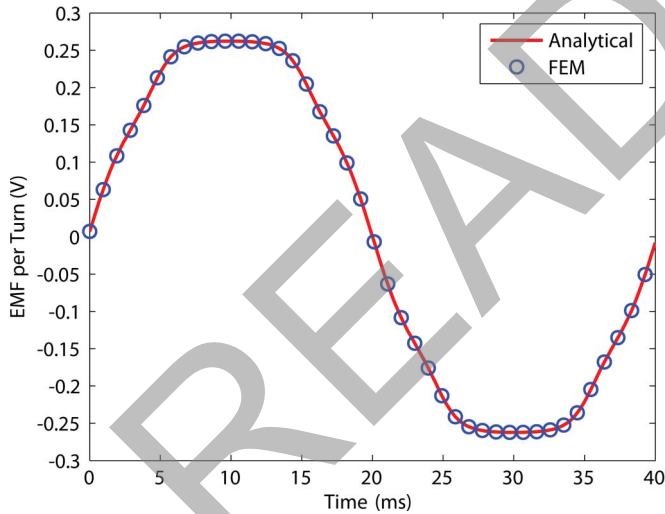


Fig. 5. Flux density distribution in the PMLSM in terms of Tesla.

Fig. 6. Flux density distribution as a function of  $x$  at the center of the air gap.Fig. 7. EMF per turn at  $v_s = 2.1$  m/s of the PMLSM.

### III. OPTIMAL DESIGN OF S<sup>3</sup>MPS

The procedure for any optimization is to find a vector  $X = (x_1, x_2, \dots, x_n)$ , representing a set of  $n$  design variables, with each of them bounded by  $x_{i_{\min}} \leq x_i \leq x_{i_{\max}}$ , with  $i = 1, 2, \dots, n$ , so that the objective function  $F(X)$  is maximized (or minimized), subject to a set of  $k$  constraints  $G_j(X) \leq 0$ , with  $j = 1, 2, \dots, k$ . As the genetic algorithm is widely used to optimize electromagnetic problems [33]–[35], in this paper, genetic algorithm is applied to the design of PMLSM to reach an air-gap flux density distribution close to sinusoidal form.

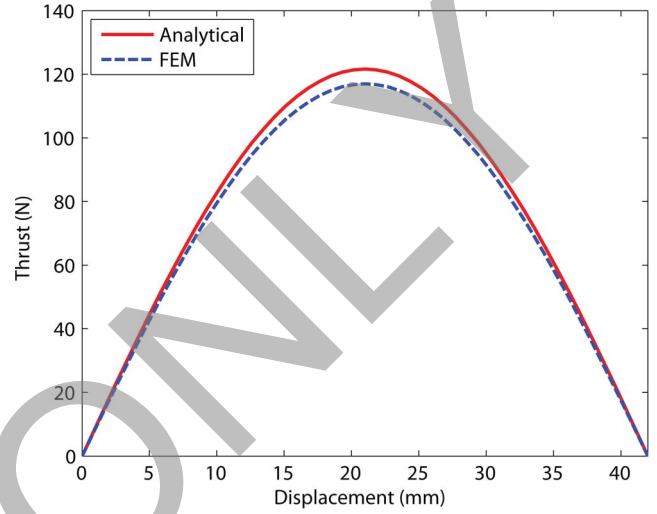
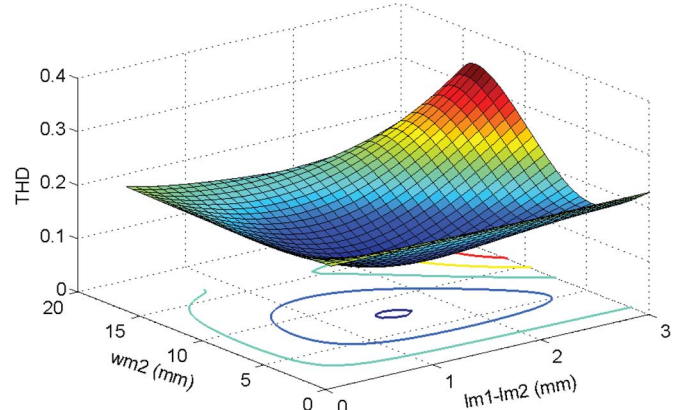


Fig. 8. Thrust characteristic of the PMLSM.

Fig. 9. THD variation with  $w_{m_2}$  and  $l_{m_1} - l_{m_2}$  for the PMLSM.

Total harmonic distortion (THD) of the flux density distribution is used as an objective function as

$$THD(X) = \frac{\sqrt{\sum_{n=3,5,\dots}^{\infty} B_{yn}^2}}{B_{y1}}. \quad (26)$$

The optimization procedure is employed to minimize the THD. Magnet dimensions are chosen as the optimization variables.

Fig. 9 shows the variation of THD in the analyzed PMLSM with two-step PM poles in terms of  $w_{m_2}$  and  $l_{m_1} - l_{m_2}$  while  $l_{m_1}$  and  $w_{m_1} + w_{m_2}$  are fixed. It is seen that an air-gap flux density distribution close to sinusoidal form can be obtained by choosing appropriate width and height of each step in the PM poles.

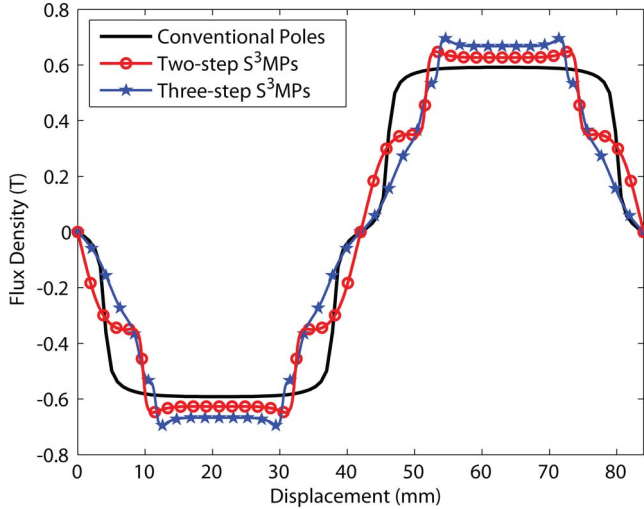


Fig. 10. Air-gap flux density distribution of the PMLSM.

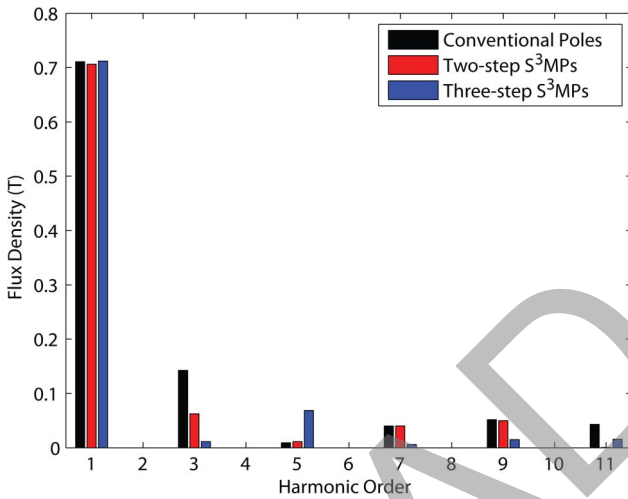


Fig. 11. Harmonics of the air-gap flux density distribution.

Figs. 10 and 11 also show the waveform and THD of the normal flux density component as a function of  $x$  position in the conventional, two-step, and three-step magnetic poles, whose parameters are presented in Table I. It is seen that the number of steps effectively influences the THD. The more the steps that the  $S^3$ MPs have, the more that the THD decreases, but the more the complexity in the manufacturing of this kind of PMLSM that the designer encounters. Therefore, in this paper, PM machines with only two and three steps are selected for investigation.

The results, shown in Figs. 9–11, confirm the need for design optimization to achieve sinusoidal distribution of flux density by choosing appropriate PM dimensions. Finding the optimal dimensions of  $S^3$ MPs with the direct search method is extremely cumbersome and would take a long time. Therefore, a genetic algorithm has been employed for the optimization procedure.

This technique consists of three basic operators, i.e., selection, crossover, and mutation. After initial population is randomly generated, the genetic algorithm operators are applied to the population to reduce their cost gradually. The roulette wheel selection is used for reproducing the population.

TABLE II  
DESIGN VARIABLES AND CONSTRAINTS

Parameter	Change Range
$2(mm) \leq l_{m_j} \leq l_{m_{j-1}} \leq \dots \leq l_{m_i} \leq \dots$	$\dots \leq l_{m_2} \leq l_{m_1} \leq 6.5(mm)$
$20(mm) \leq 2w_{m_j} + 2w_{m_{j-1}} + \dots$	$\dots + 2w_{m_i} + \dots + 2w_{m_2} + w_{m_1} \leq 42(mm)$
	$120(N) \leq F_{avg} \leq 122(N)$

TABLE III  
PARAMETERS OF THE OPTIMIZED  $S^3$ MPs

Parameter	Motor Types			
	Two-step $S^3$ MPs		Three-step $S^3$ MPs	
$l_m(mm)$	$l_{m_1}$	5.9	$l_{m_1}$	6.1
	$l_{m_2}$	4.5	$l_{m_2}$	5.4
			$l_{m_3}$	4
$w_m(mm)$	$w_{m_1}$	17	$w_{m_1}$	12.7
			$w_{m_2}$	4.5
	$w_{m_2}$	7.7	$w_{m_3}$	6.2

The following values of genetic operators are used in the genetic algorithm:

- 1) initial population:  $N = 50$ ;
- 2) probability of mutation:  $P_m = 0.07$ ;
- 3) probability of crossover:  $P_c = 0.07$ ;
- 4) number of generations:  $N_g = 1000$ .

To have a more realistic design, some limitations are applied to the optimization procedure, as shown in Table II. Finally, in the optimal models, PM dimensions calculated using the genetic algorithm are listed in Table III.

#### IV. DESIGN EVALUATION

The performance of the optimized PMLSMs is investigated and compared with the performance of the initial PMLSMs with the specifications listed in Table I. Since an optimization procedure based on the analytical method has been employed to determine the optimal design specifications, another method with higher accuracy, for example, the FEM, should be used to assess the performance of the optimized motors.

The flux density distributions produced by the PM poles of the optimal designs and initial machines in the middle of the mechanical air gap calculated by FEM are shown in Figs. 12 and 13. The harmonic contents of the flux density distribution for both initial and optimized motors are also shown in Figs. 14 and 15. It can be seen that the harmonics in the optimized motor reduce substantially. In the two-step  $S^3$ MPs, the THD reduces from 14% in the initial motor to 9.1% in the optimal one, while in the three-step  $S^3$ MPs, the THD decreases from 10.6% in the initial motor to 5.2% in the optimized one.

Moreover, the EMF waveforms at the nominal speed obtained by FEM are shown in Figs. 16 and 17. The fundamental component amplitudes of the EMF curves of the optimized motor are calculated and used as the amplitudes of the standard sinusoidal waveforms. It is also observed that the mismatch between the standard sinusoidal curves and EMF waveforms of the optimal motors is approximately zero.

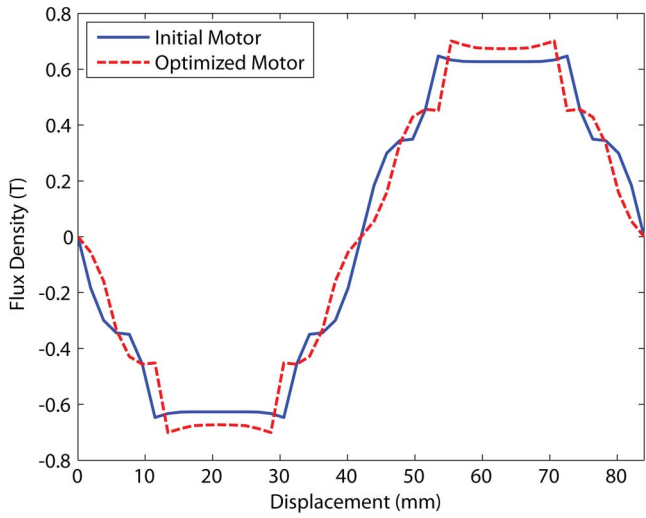


Fig. 12. Air-gap flux density distribution of the two-step S<sup>3</sup>MPs in the PMLSM.

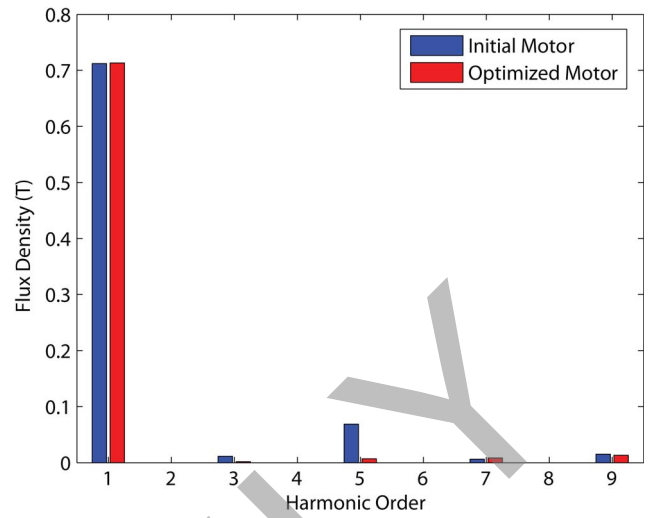


Fig. 15. Harmonics of the air-gap flux density distribution of the three-step S<sup>3</sup>MPs in the PMLSM.

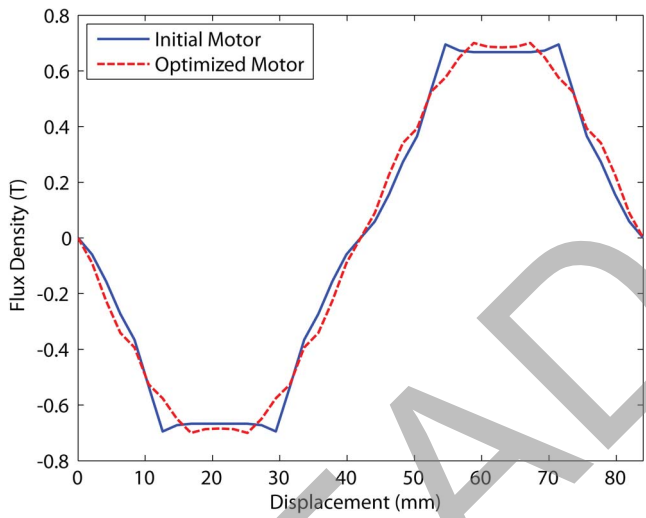


Fig. 13. Air-gap flux density distribution of the three-step S<sup>3</sup>MPs in the PMLSM.

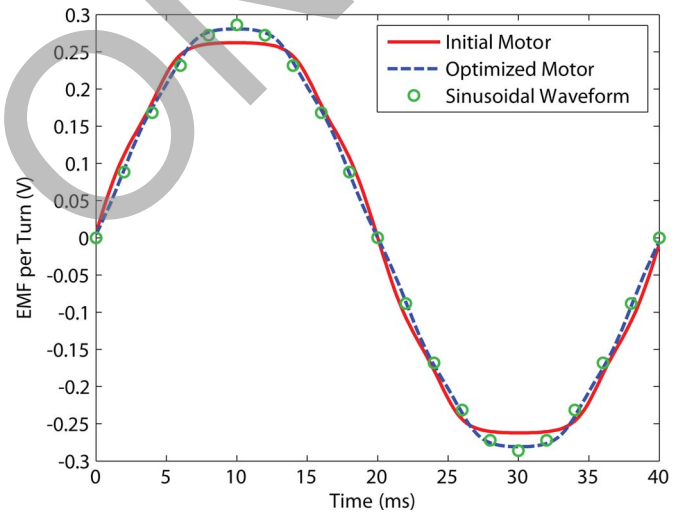


Fig. 16. EMF of the two-step S<sup>3</sup>MPs in the PMLSM.

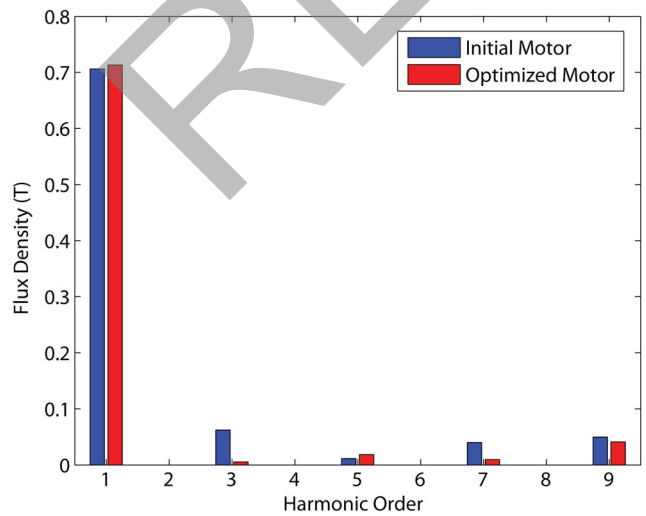


Fig. 14. Harmonics of the air-gap flux density distribution of the two-step S<sup>3</sup>MPs in the PMLSM.

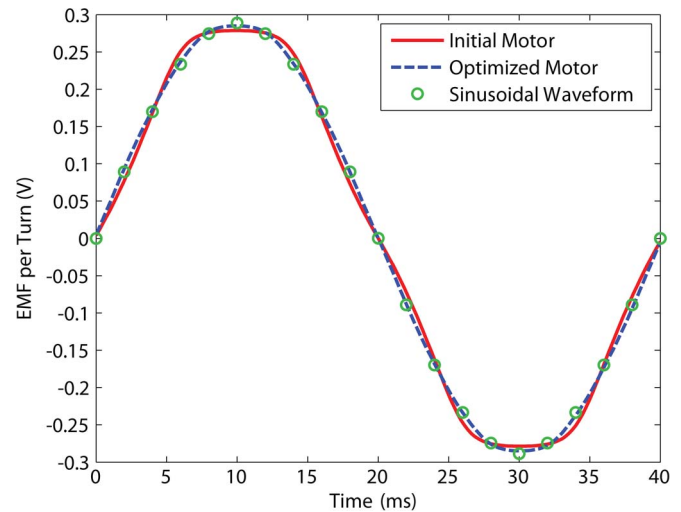


Fig. 17. EMF of the three-step S<sup>3</sup>MPs in the PMLSM.

## V. CONCLUSION

As PMLSMs offer many advantages for the applications of EML, this paper has proposed an S<sup>3</sup>MP structure for enhancing the performance of PMLSMs. An analytical analysis has been presented to model the air-gap flux density distribution, EMF, and thrust in the PMLSM with S<sup>3</sup>MPs. The analytically calculated results have been evaluated using FEM. The close agreement between the results of two methods confirms the effectiveness of the presented model. Thus, there is no need to apply the time-consuming FEM for design optimization. The pole shape optimization for two PMLSMs with two types of S<sup>3</sup>MPs has been then carried out using the analytical model and genetic algorithm. Finite-element analysis results show that the optimization procedure significantly reduces the flux density as well as the EMF harmonics.

## REFERENCES

- [1] L. Li, M. Ma, B. Kou, and Q. Chen, "Analysis and optimization of slotless electromagnetic linear launcher for space use," *IEEE Trans. Plasma Sci.*, vol. 39, no. 1, pp. 127–132, Jan. 2011.
- [2] K. Baoquan, L. Liyi, and Z. Chengming, "Analysis and optimization of thrust characteristics of tubular linear electromagnetic launcher for space-use," *IEEE Trans. Magn.*, vol. 45, no. 1, pp. 250–255, Jan. 2009.
- [3] L. Li, M. Ma, B. Kou, and Q. Chen, "Analysis and design of moving-magnet-type linear synchronous motor for electromagnetic launch system," *IEEE Trans. Plasma Sci.*, vol. 39, no. 1, pp. 121–126, Jan. 2011.
- [4] Q. Wang, J. Zou, J. Zou, and M. Zhao, "Analysis and computer-aided simulation of cogging force characteristic of a linear electromagnetic launcher with tubular transverse flux machine," *IEEE Trans. Plasma Sci.*, vol. 39, no. 1, pp. 157–161, Jan. 2011.
- [5] W. Zhu, B. Fahimi, and S. Pekarek, "A field reconstruction method for optimal excitation of permanent magnet synchronous machines," *IEEE Trans. Energy Convers.*, vol. 21, no. 2, pp. 305–313, Jun. 2006.
- [6] J. A. Guemes, A. M. Iraolagoitia, J. I. Del Hoyo, and P. Fernandez, "Torque analysis in permanent-magnet synchronous motors: A comparative study," *IEEE Trans. Energy Convers.*, vol. 26, no. 1, pp. 55–63, Mar. 2011.
- [7] L. Liyi, J. Hong, Z. Lu, L. Ying, Y. Song, L. Rizhong, and L. Xiaopeng, "Fields and inductances of the sectioned permanent-magnet synchronous linear machine used in the EMALS," *IEEE Trans. Plasma Sci.*, vol. 39, no. 1, pp. 87–93, Jan. 2011.
- [8] M. Mirzaei, S. E. Abdollahi, and H. Lesani, "A large linear interior permanent magnet motor for electromagnetic launcher," *IEEE Trans. Plasma Sci.*, vol. 39, no. 6, pp. 1566–1570, Jun. 2011.
- [9] L. Li, H. Xuzhen, P. Donghua, and C. Jiwei, "Magnetic field of a tubular linear motor with special permanent magnet," *IEEE Trans. Plasma Sci.*, vol. 39, no. 1, pp. 83–86, Jan. 2011.
- [10] S. Vaez-Zadeh and A. H. Isfahani, "Multiobjective design optimization of air-core linear permanent-magnet synchronous motors for improved thrust and low magnet consumption," *IEEE Trans. Magn.*, vol. 42, no. 3, pp. 446–452, Mar. 2006.
- [11] M. F. Hsieh and Y. S. Hsu, "An investigation on influence of magnet arc shaping upon back electromotive force waveforms for design of permanent-magnet brushless motors," *IEEE Trans. Magn.*, vol. 41, no. 10, pp. 3949–3951, Oct. 2005.
- [12] Y. Li, J. Xing, T. Wang, and Y. Lu, "Programmable design of magnet shape for permanent magnet synchronous motors with sinusoidal back-EMF waveforms," *IEEE Trans. Magn.*, vol. 44, no. 9, pp. 2163–2167, Sep. 2008.
- [13] Y. Li, J. Zou, and Y. Lu, "Optimum design of magnet shape in permanent-magnet synchronous motors," *IEEE Trans. Magn.*, vol. 39, no. 6, pp. 3523–3526, Nov. 2003.
- [14] P. Zheng, J. Zhao, J. Han, J. Wang, Z. Yao, and R. Liu, "Optimization of the magnetic pole shape of a permanent-magnet synchronous motor," *IEEE Trans. Magn.*, vol. 43, no. 6, pp. 2531–2533, Jun. 2007.
- [15] S. Chaithongsuk, N. Takorabet, and F. Meibody-Tabar, "On the use of pulse width modulation method for the elimination of flux density harmonics in the air gap of surface PM motors," *IEEE Trans. Magn.*, vol. 45, no. 3, pp. 1736–1739, Mar. 2009.
- [16] A. H. Isfahani, "Analytical framework for thrust enhancement in permanent-magnet (PM) linear synchronous motors with segmented PM poles," *IEEE Trans. Magn.*, vol. 46, no. 4, pp. 1116–1122, Apr. 2010.
- [17] A. H. Isfahani, S. Vaez-Zadeh, and M. A. Rahman, "Using modular poles for shape optimization of flux density distribution in permanent magnet machines," *IEEE Trans. Magn.*, vol. 44, no. 8, pp. 2009–2015, Aug. 2008.
- [18] K. J. Meessen, B. L. J. Gysen, J. J. H. Paulides, and E. A. Lomonova, "Halbach permanent magnet shape selection for slotless tubular actuators," *IEEE Trans. Magn.*, vol. 44, no. 11, pp. 4305–4308, Nov. 2008.
- [19] J. S. Choi and J. Yoo, "Design of a Halbach magnet array based on optimization techniques," *IEEE Trans. Magn.*, vol. 44, no. 10, pp. 2361–2366, Oct. 2008.
- [20] M. Markovic and Y. Perriard, "Optimization design of a segmented Halbach permanent-magnet motor using an analytical model," *IEEE Trans. Magn.*, vol. 45, no. 7, pp. 2955–2960, Jul. 2009.
- [21] Y. Yang, X. Wang, R. Zhang, T. Ding, and R. Tang, "The optimization of pole arc coefficient to reduction cogging torque in surface-mounted permanent magnet motors," *IEEE Trans. Magn.*, vol. 42, no. 4, pp. 1135–1138, Apr. 2006.
- [22] M. Y. Kim, Y. C. Kim, and G. T. Kim, "Design of slotless-type PMLSM for high power density using divided PM," *IEEE Trans. Magn.*, vol. 40, no. 2, pp. 746–749, Mar. 2004.
- [23] S. M. Jang, S. H. Lee, and I. K. Yoon, "Design criteria for detent force reduction of permanent-magnet linear synchronous motors with Halbach array," *IEEE Trans. Magn.*, vol. 38, no. 5, pp. 3261–3263, Sep. 2002.
- [24] P. S. Shin, S. H. Woo, Y. Zhang, and C. S. Koh, "An application of Latin hypercube sampling strategy for cogging torque reduction of large-scale permanent magnet motor," *IEEE Trans. Magn.*, vol. 44, no. 11, pp. 4421–4424, Nov. 2008.
- [25] M. Ashabani and Y. A. I. Mohamed, "Multiobjective shape optimization of segmented pole permanent-magnet synchronous machines with improved torque characteristics," *IEEE Trans. Magn.*, vol. 47, no. 4, pp. 795–804, Apr. 2011.
- [26] S. Kim, J. Hong, Y. Kim, H. Nam, and H. Cho, "Optimal design of slotless-type PMLSM considering multiple responses by response surface methodology," *IEEE Trans. Magn.*, vol. 42, no. 4, pp. 1219–1222, Apr. 2006.
- [27] J. K. Kim, S. W. Joo, S. C. Hahn, J. P. Hong, D. H. Kang, and D. H. Koo, "Static characteristics of linear BLDC motor using equivalent magnetic circuit and finite element method," *IEEE Trans. Magn.*, vol. 40, no. 2, pp. 742–745, Mar. 2004.
- [28] A. H. Isfahani and S. Vaez-Zadeh, "Design optimization of a linear permanent magnet synchronous motor for extra low force pulsations," *Energy Conv. Manag.*, vol. 48, no. 2, pp. 443–449, Feb. 2007.
- [29] N. Chayopitak and D. G. Taylor, "Performance assessment of air-core linear permanent-magnet synchronous motors," *IEEE Trans. Magn.*, vol. 44, no. 10, pp. 2310–2316, Oct. 2008.
- [30] Z. Q. Zhu, Z. P. Xia, L. J. Wu, and G. W. Jewell, "Analytical modeling and finite-element computation of radial vibration force in fractional-slot permanent-magnet brushless machines," *IEEE Trans. Ind. Appl.*, vol. 46, no. 5, pp. 1908–1918, Sep./Oct. 2010.
- [31] J. Wang, G. W. Jewell, and D. Howe, "A general framework for the analysis and design of tubular linear permanent magnet machines," *IEEE Trans. Magn.*, vol. 35, no. 3, pp. 1986–2000, May 1999.
- [32] J. Wang and D. Howe, "Design optimization of radially magnetized, iron-cored, tubular permanent magnet machines and drive systems," *IEEE Trans. Magn.*, vol. 40, no. 5, pp. 3262–3277, Sep. 2004.
- [33] H. Li, Z. Chen, and H. Polinder, "Optimization of multibrid permanent-magnet wind generator systems," *IEEE Trans. Energy Convers.*, vol. 24, no. 1, pp. 82–92, Mar. 2009.
- [34] H. M. Hasani, A. S. Abd-Rabou, and S. M. Sakr, "Design optimization of transverse flux linear motor for weight reduction and performance improvement using response surface methodology and genetic algorithms," *IEEE Trans. Energy Convers.*, vol. 25, no. 3, pp. 598–605, Sep. 2010.
- [35] K. T. Chau, Q. Sun, Y. Fan, and M. Cheng, "Torque ripple minimization of doubly salient permanent-magnet motors," *IEEE Trans. Energy Convers.*, vol. 20, no. 2, pp. 352–358, Jun. 2005.



**Nariman Roshandel Tavana** (S'08) was born in Rasht, Iran, in 1983. He received the B.Sc. degree in electrical engineering from The University of Guilan, Rasht, in 2006 and the M.Sc. degree (with honors) in electrical power engineering (power electronics and electric machines) from the Iran University of Science and Technology, Tehran, Iran, in 2009. He is currently working toward the Ph.D. degree in the Department of Electrical and Computer Engineering, University of Alberta, Edmonton, AB, Canada.

His research interests include design and modeling of electrical machines, finite-element analysis of electromagnetic devices, motor drives, and real-time simulation of electrical machines and power electronics.



**Venkata Dinavahi** (S'94–M'00–SM'08) received the Ph.D. degree in electrical and computer engineering from the University of Toronto, Toronto, ON, Canada, in 2000.

He is a Professor with the University of Alberta, Edmonton, AB, Canada. His research interests include real-time simulation of electrical machines, power electronics, and power systems, large-scale system simulation, and parallel and distributed computing.



**Abbas Shoulaie** was born in Isfahan, Iran, in 1949. He received the B.Sc. degree from the Iran University of Science and Technology (IUST), Tehran, Iran, in 1973 and the M.Sc. and Ph.D. degrees in electrical engineering from the Universite des Sciences et Technologies de Lille 1, Montpellier, France, in 1981 and 1984, respectively.

He is currently a Full Professor of electrical engineering with IUST. His current research interests include power electronics, magnetic systems and linear machines, flexible alternating-current transmission system devices, and HVDC.

READ ONLY